



The influence of fibre orientation in self-compacting concrete on 4-point bending strength

Heiko Herrmann^{a*}, Oksana Goidyk^a, Hendrik Naar^b, Tanel Tuisk^b, and Andres Braunbrück^a

^a Department of Cybernetics, Tallinn University of Technology, Akadeemia tee 21, 12618 Tallinn, Estonia

^b Department of Civil Engineering and Architecture, Tallinn University of Technology, Ehitajate tee 5, 19086 Tallinn, Estonia

Received 13 December 2018, accepted 2 March 2019, available online 15 August 2019

© 2019 Authors. This is an Open Access article distributed under the terms and conditions of the Creative Commons Attribution-NonCommercial 4.0 International License (<http://creativecommons.org/licenses/by-nc/4.0/>).

Abstract. This contribution presents the performed experiments and experimental setup in detail for future reference and the results of bending tests performed on steel fibre concrete beam specimen, which have been cut out of a larger plate. These beams have different fibre orientation distributions, due to being taken from different parts of the plate and with different orientation with respect to the flow of the fresh concrete.

Key words: mechanics, fibre orientation, bending test, fibre concrete, strength analysis.

1. INTRODUCTION

With the shortage of sand and gravel in many areas [1] and the global concern about carbon dioxide emissions, it becomes necessary to reduce the environmental impact of concrete construction. Concrete is an ubiquitous building material, it is also essential for wind farms [2], which are the main providers of renewable energy. One possibility to achieve this is to create stronger concrete that behaves ductile. The addition of short fibres to the concrete mix can introduce ductility to concrete. However, the results of strength tests on small test-specimen show great variability and the test results of large elements do not match the results of the strongest small specimen. The probable causes for the variability are the spatial fibre distribution and the orientational fibre distribution, which can both vary between small specimen and also within a large element [3,4]. Fibre pullout tests have shown, that the pullout force depends on the inclination angle of the fibre. The angle between fibre and crack therefore influences the post-cracking behaviour [5,6]. Theoretical approaches that model the dependence of the mechanical properties and take the fibre orientations into account

have been proposed by several research teams, the used methods range from orientation numbers over orientation profile to orientation tensors [7–12]. Both, for comparison of experiments and for application of the theories it is necessary to know the fibre orientations. Fibre orientation measurements can be performed using X-ray computed tomography [3,13–23], which gives the orientations and positions of individual fibres, and by electro-magnetic methods, which give tendencies of fibre alignment. A comparison of different measurement techniques can be found in [24].

The spatial variation of fibre density and orientation distribution within a structural element is largely due to the flow of the fresh concrete mass when filling the formwork [25–30]. In this study the experiments to determine the local strength characteristics of a large plate are presented. The aim is to correlate the strength characteristics with fibre orientations expected from casting simulations. To achieve this, a large plate was cast with documented casting procedure and the plate was cut into beams, which have been subjected to four-point bending tests. The post-cracking behaviour of beams has also been studied by other researchers, e.g., using three-point bending tests of unnotched specimen

* Corresponding author, hh@cens.ioc.ee

[30–32]. This paper focuses on the description of experiments and the presentation of the raw results from the bending tests. The detailed analysis of the measurements is left for a future paper.

2. EXPERIMENTS

In this section the experiment setup is described, first a description of the casting of the fibre concrete and reference plates including the concrete mix is given, then the setting of the four-point bending tests is described, followed by digital image correlation and acoustic emission measurements, that have been performed during some of the bending tests.

2.1. Casting of plates, materials and mix design

For this study, two different mixtures: an ordinary self-compacting concrete (SCC) and steel fibre reinforced self-compacting concrete (SFRSCC), were produced according to the recipe by the manufacturer. The composition of the mixtures is presented in Table 1. The constituent materials were mixed according to normal factory procedure in a production-line mixer with a capacity of 1–2 t.

The consistency and viscosity of the concrete mixture was measured by means a slump-flow test, according to EN12350-8. The spread of the slump was 700 mm, which satisfied the requirement of 650–800 mm.

In the end, the obtained mixture was placed into the previously prepared film coated plywood mould, whose bottom was covered with plastic foil. As filling method a moving bucket was used, the pouring position was moved in the longitudinal direction.

For the second mixture the same recipe and procedure were used. However, this time hooked-end steel fibres were added. Table 2 provides the characteristics and properties of used steel fibres, a photo of a fibre is presented in Fig. 1. To avoid clustering of fibres the mixture was mixed for a couple of minutes. The fibre dosage was 1% per volume of concrete. To achieve the required rheological properties of the concrete mixture, the water dosage was slightly increased. After the slump flow test (spread of the slump was 650 mm), the same casting procedure was performed. To provide the accurate surface leveling the surface was treated with a roller immediately after the casting process. After both casting processes lifting anchors were put into the fresh concrete, to be able to transport the plate safely after hardening. The videos of both casting processes were recorded with a camera for further visual observation and analysis. Then both slabs were stored in the manufacturing hall at room temperature and left to harden.

Standard compression tests have been performed on separately cast cubic test specimen, the concrete for these was taken out of the mass for the plates during casting.

Table 1. Composition of SCC mix, amount mixed: 1 m³

Cement, kg	330
Sand (0–2 mm), kg	398
Sand (0–4 mm), kg	505
Crushed stone (2–5), kg	336
Crushed stone (8–11), kg	539
Filler, kg	80
Admixture, kg	5.1
Water, kg	175
Fibres (SFSCC only), kg	50
Extra water (SFSCC only), kg	~10

Table 2. Data of the steel fibres, according to [33]

Manufacturer	Severstal Metiz
Model	Hendix prime 75/52
Type	Hooked end
Length, mm	52 ± 2.0
Diameter, mm	0.75 ± 0.04
Hook length, mm	2.0 – 1.0/ + 2.0
Hook height, mm	2.1 + 0.5/ – 0.0
Bend angle, degrees	40 ± 5
Tensile strength, MPa	1500
Elastic modulus, MPa	≥ 190 000
Number of fibres per kg, pcs.	~ 5 545



Fig. 1. Photo of a fibre.

2.2. Preparation of beam specimen

After hardening and demoulding both slabs had dimensions of ($L \times W \times H$) 400 cm × 100 cm × 10 cm. From the slab of SCC 10 beams of size 100 cm × 10 cm × 10 cm have been cut. The slab of SFRSCC has been cut into 40 beams of size 100 cm × 10 cm × 10 cm. A principal layouts of the specimens cut out of the cast slabs is presented in Fig. 2. The cutting of both plates took place twenty days after the casting.

2.3. The bending test set-up

The main goals of 4-point bending test are to evaluate the tensile and post-cracking behaviour of SFRSCC, determine the peak load, the mid-span deflections, crack mouth opening displacement and the contribution of fibres in the strength of fibre concrete. The basic idea to carry out 4-point bending test with unnotched specimens is concerned with the evaluation of the

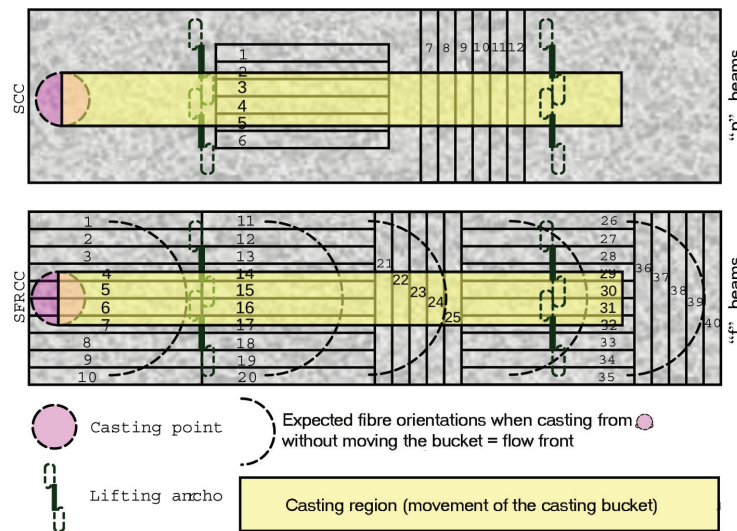


Fig. 2. Beam layout of specimens cut out of the cast plates; SFRCC beams are referred to with “f” and their number, non-fibre beams with “p” and their number.

influence of fibre distribution on independent crack formation/propagation and post-cracking behaviour, since generally, the existence of the notch in the midspan section would modify the stress pattern and anticipates the formation and further growing of the crack.

All the 50 beams were subjected to 4-point bending test in order to analyse and compare the mechanical properties and the post-cracking behaviour of concrete.

The 4-point bending test of specimens was performed on a universal electro-mechanic/hydraulic testing machine *EU100*. The testing machine was connected to an *HBM QuantumX MX840A* universal measuring amplifier module to acquire the data and a laptop to record the experimental data and control the testing procedure. For the data collection and visualization the *CatmanEasy DAQ* software was used.

The experimental equipment and the concrete specimen mounted in the testing machine is depicted in Fig. 3a (photo) and Fig. 3b (drawing).

The beams were maintained by means of two supports with the metal rollers at the edges with a diameter of 5 cm. Two metal plates were located on the top of the rollers in order to fix and eliminate any movements of the testing specimens. The distance between supports was 90 cm, and 5 cm from each supports to the edges of the beams. The experimental beams were correctly centered with the supports of the testing machine. The load was applied through two metal cylinders of 1.5 cm diameter located between two metal plates of size 2 cm × 1 cm and length 15 cm in order to ensure the stability and evenly distribute of the loading force. The loading points were located at the distance

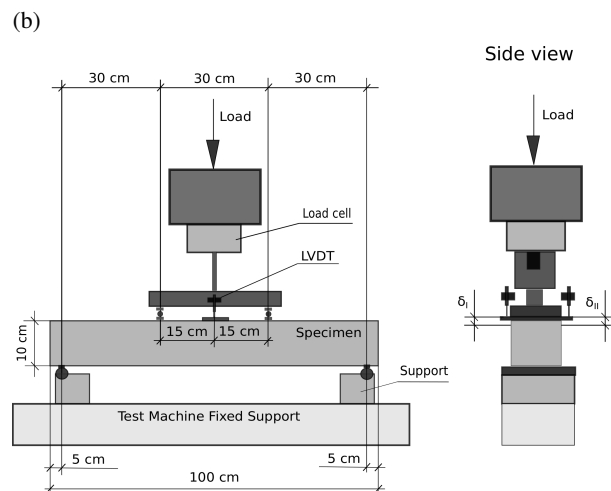


Fig. 3. Four point bending test: (a) photo of the setup, (b) sketch.

of 30 cm from each other (approximately 1/3 of total range). To measure the loading force during the test, the load cell *HBM U10M* with a capacity of 50 kN was used. The displacement was continuously increased until the displacements achieved specific values. The maximum load for all specimens was in the range 6–8 kN.

The accurate measurements and recording of the mid-span deflections during the bending test were arranged. To determine the vertical displacements under the load, the displacement sensors *HBM W1/10mm-T* were applied. The displacement sensors were located on a metal plate at half-length on the top surface of the specimen and fixed on two opposite sides of specimen (δ_I , δ_{II}). The displacement transducers have to be carefully mounted in order to exclude the rotation. The schematic illustration of the displacement transducers is shown in Fig. 3b.

In order to get the accurate measurements it is important before the test to make sure that the surface of the specimens are clean and free of the industrial dust and other extraneous materials. At the time of the bending tests the samples have been between 23 weeks and 28 weeks old. This means that all specimen have been over five months old at the time of testing and the effect of the difference in age at the time of testing should be negligible.

2.4. The digital image correlation set-up

Digital image correlation (DIC) method is an effective optical and non-contact measuring technique that employs the comparing, tracking the changes and visualization of deformations in the digital images of the specimen surface. The main principle of this method is based on digital image processing and numerical computing that involves monitoring and identifying transformations in a surface pattern of objects under the loading [34–37].

The most important step during the experimental setup is the appropriate arrangement of the specimen, camera and light sources. Since the obtained results strongly depend on the quality of the images, the equipment disposition should be organized quite thoroughly. Primarily, the camera should be positioned exactly in front of the specimen at sufficient distance and perpendicularly to the main axis of the specimen. The light sources (white or natural day light can be used) play a significant role because it enhances the contrast and therefore, the quality of the final images.

In the research, to record the video and images of the testing beams a digital camera with a photo-resolution of 4608×3456 pixels and a HD video-resolution of 1280×720 pixels was used. The digital camera was mounted on a tripod, perpendicular to one side of the specimen and accurately directed to the area of interest. The distance from the camera to the testing specimen was approximately 60 cm. The schematic illustration of the experimental setup for DIC is presented in Fig. 4.

For DIC analysis the software package *pydic* [38] was used. *Pydic* is a free and easy-to-use software for

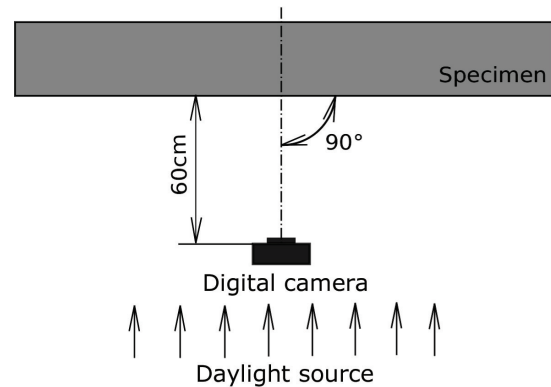


Fig. 4. The typical experimental setup for digital image correlation (top view).

computing the displacement and the strain fields inside a region of interest, that is based on Python packages. The testing images were obtained as screen-shots from the video. Generally, DIC analysis involves the comparison of the images that were taken upon the bending test, before, during and after the deformation process caused by the applied force. In other words, DIC software computes and traces the position changes of each image point by comparing several images of object surface in various moment in time. For DIC analysis each experimental image was converted from RGB colour to grayscale (eight-bit digital images). Moreover, it is required that among the testing images the first one should be taken in undeformed state and another during deformed state.

Figures 5a and 5b show the typical images used for DIC in different states of the specimen.

2.5. The acoustic emission set-up

The acoustic emission (AE) method is widespread non-destructive technique assigned to investigate the internal and external damages in the materials.

Under the applied load the localized stress energy causes the crack appearance and growing/propagation that induces sound waves. These waves can be extracted and recorded by using transducers (sensors) or microphones, mounted on the surface of the testing specimens [39]. As a result, AE signal parameters, such as amplitude, counts, energy, duration time, rise time are obtained by the measurement system and further used for the post-processing analysis [40,41].

The intention to use record AE was to try to identify which crack appeared first in case of multi-cracking and to possibly identify fibre-rupture events.

The schematic experimental setup and positions of microphones that were used for the AE technique are presented in Fig. 6.

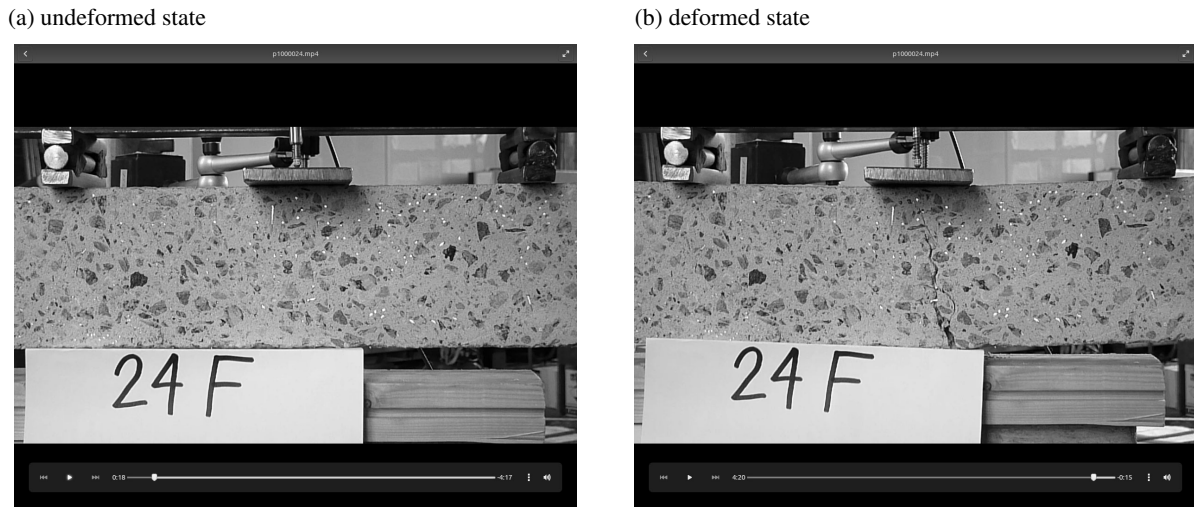


Fig. 5. Typical photos used for digital image correlation (undeformed and deformed state).

Two piezo clip-on contact microphones were attached to the metal plates, located between bottom of the specimen and rollers of supports. It is worth to note, that the economic contact microphones were not matched and their sensitivity varied considerably. This was compensated by the level setting of the microphone pre-amps in the audio interface. A matched stereo pair of compact condenser microphones was mounted on two tripods at the distance about 10 cm from the opposite side of the specimen. The AE signals were recorded with a four-channel USB Audio Interface, the amplitude resolution was 24 bit and time resolution for the initial recordings 192 kHz and later reduced to 96 kHz because of the file size and software crashes. The audio interface was connected to a Linux laptop (Debian Linux stretch) running the JACK audio daemon [42] and Ardour5.5.0 [43] recording software. The JACK daemon

proved superior to using Ardour5.5.0 with ALSA [44], because in the case of xruns (buffer under/over-runs) the recording continued when using the JACK daemon, while it was stopped when using the Ardour5.5.0 ALSA driver. For later recordings only the contact microphones were used, as these have been resistant to ambient noise and due to other experiments in the same hall, the ambient noise level had increased over the duration of the experiments.

To synchronize the audio recording with the load-displacement measurements, after switching all recordings on, the plate on which the displacement sensors where in contact with the beam was hit slightly with a metal rod. This caused a very small temporary displacement and an audible ping. Both were recorded and can be used for synchronization.

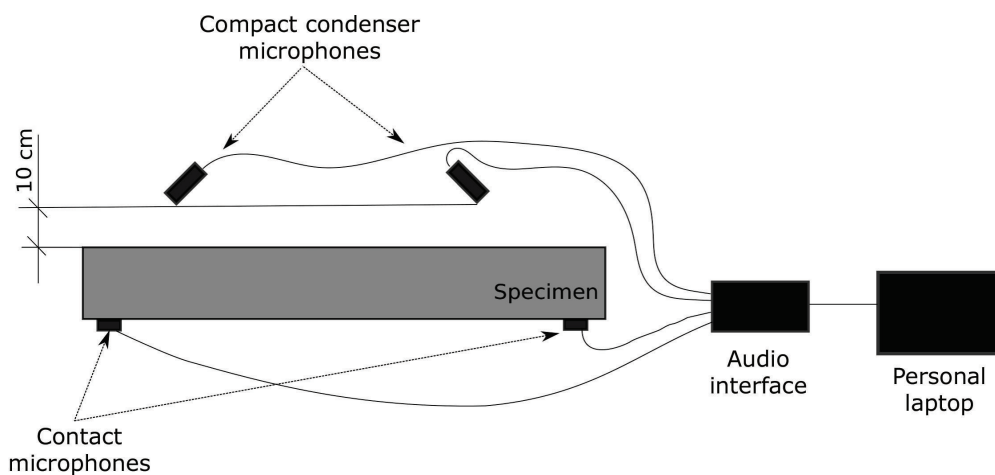


Fig. 6. An experimental setup for acoustic emission monitoring.

3. RESULTS

In the following, the results of the experiments are presented. In particular, the load-displacement curves for all beams are given, and a proof-of-concept for the digital image correlation and acoustic emission measurements. A detailed analysis of the results is ongoing and will be presented elsewhere.

3.1. The compression tests

The results of the compression tests are presented in Table 3. It is notable, that the normal concrete without fibres shows higher strength at all ages compared to the fibre concrete. This can partly be explained by the higher water-cement ratio of the fibre concrete.

3.2. The bending tests

Here the load-displacement diagrams of the four-point bending test are presented in Fig. 7. One can notice that the variation between the different beams is large, though in all cases the presence of the fibres introduced some ductility into the concrete. The range of post-cracking behaviour included strain hardening cases, where the

maximum load is higher than the load at the first crack, but also strain-softening, where the residual strength is only a quarter of the load at first crack. Some correlation between the position of the beam in the plate and the post-cracking behaviour can be observed, for example the beams taken from the edges of the plate are strain-hardening, while the middle beams show weak post-cracking strength. Many of these results are in accordance with expectations with respect to fibre orientations, however there are also cases that do not seem to agree. The analysis of these is ongoing and will be presented in a future paper.

3.3. The digital image correlation

To obtain the strain distribution images, at first, the region of interest was specified as a virtual computational grid. Further, the program calculates the displacements at the each point of this virtual grid. After the execution of the full cycle of DIC analysis, the program writes the typical series of results' files, that include the folder with images of displacements' field, the folder with images of displacements' grids, the folder with images of the displacements of the correlated windows and CSV results files that are needed for post-processing.

Table 3. Results of compression tests for SCC and SFRSCC

	Age at test in days	4	4	4	7	7	7	28	28	28	28	28	28	28	28	28	28
SCC	ρ , kg/m ³	2330	2330	2330	2310	2340	2370	2380	2380	2370	2380	2360	2380	2390	2380	2380	2390
	$\bar{\rho}$, kg/m ³		2330			2340						2379					
	stdev, kg/m ³		0			30						9					
	$\sigma_{u,c}$, MPa	55.4	54.5	52.3	54.7	54.5	56.8	67.6	66.4	70.9	66.3	68.8	69	69.9	72.1	66	69
	$\bar{\sigma}_{u,c}$, MPa		54.1			55.3						68.6					
	stdev, MPa		2			1						2					
SFRSCC	ρ , kg/m ³	2350	2350	2370	2380	2360	2370	2390	2370	2380	2380	2410	2390	2370	2390	2360	2380
	$\bar{\rho}$, kg/m ³		2357			2370						2382					
	stdev, kg/m ³		12			10						14					
	$\sigma_{u,c}$, MPa	45.1	45	44.5	46.1	45.3	45.1	55.7	55	57.2	58.1	57.3	57.4	56.9	55.9	58.1	54.9
	$\bar{\sigma}_{u,c}$, MPa		44.9			45.5						56.6					
	stdev in MPa		0			1						1					

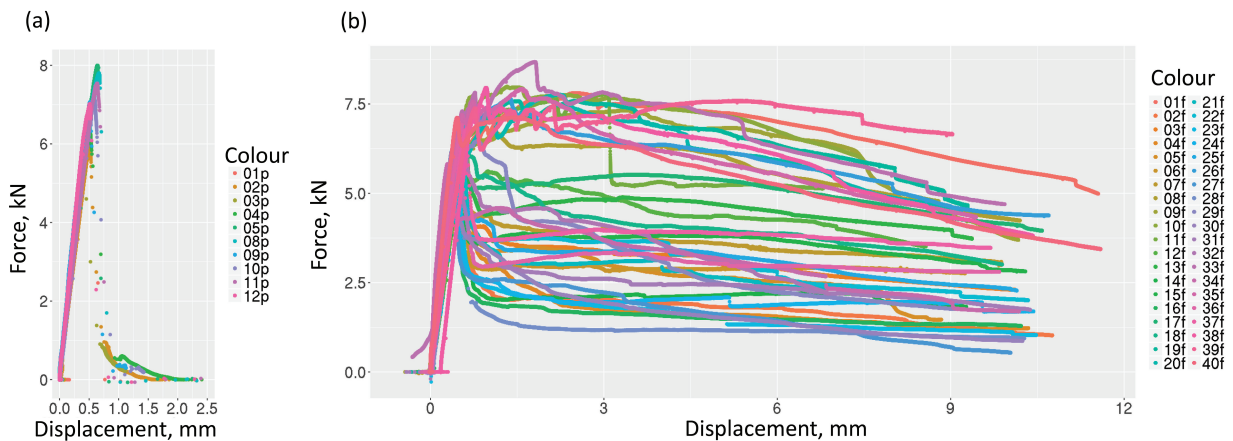


Fig. 7. Load-displacement diagrams for the tested beams: (a) SCC, (b) SFRSCC.

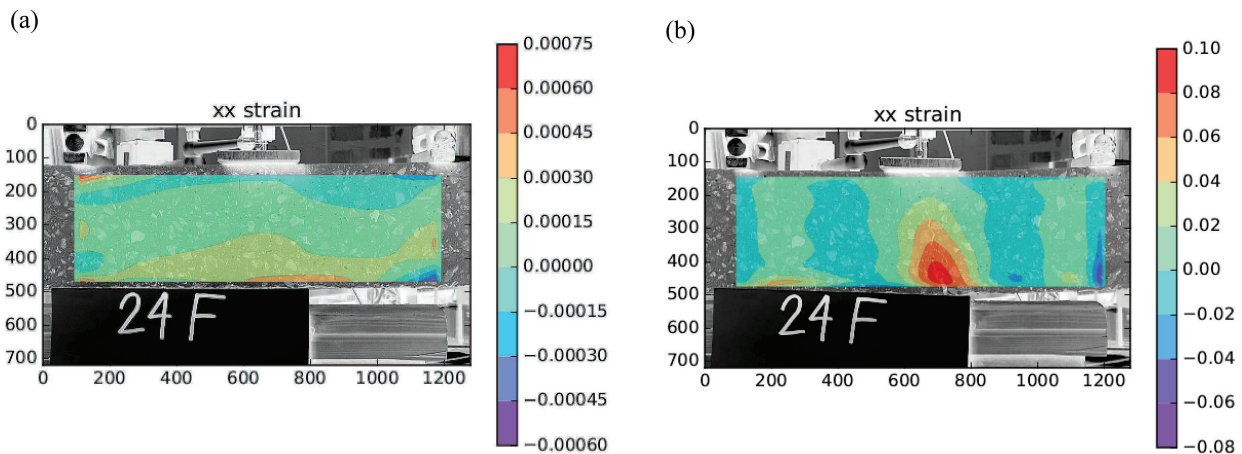


Fig. 8. Horizontal strain in beam 24f: (a) analysis just before the crack, (b) analysis after the crack.

Finally, the software allows to create plots of the strain field interactively with matplotlib, a Python library for plotting [45], see Fig. 8. Additionally, the program automatically computes the Young’s modulus from strain fields and meta-data.

3.4. The acoustic emission

The setup for recording acoustic emissions during the bending experiments was successful. Despite some

software instability, many crack events could be recorded acoustically. An example of such a recording is presented in Fig. 9. The figure shows the amplitudes over time recorded by the four microphones. As the figure shows, the noise level is very low for all microphones and the crack events can be clearly identified without further filtering techniques.

A detailed analysis of the recorded events is still under way and will be presented in a different publication.

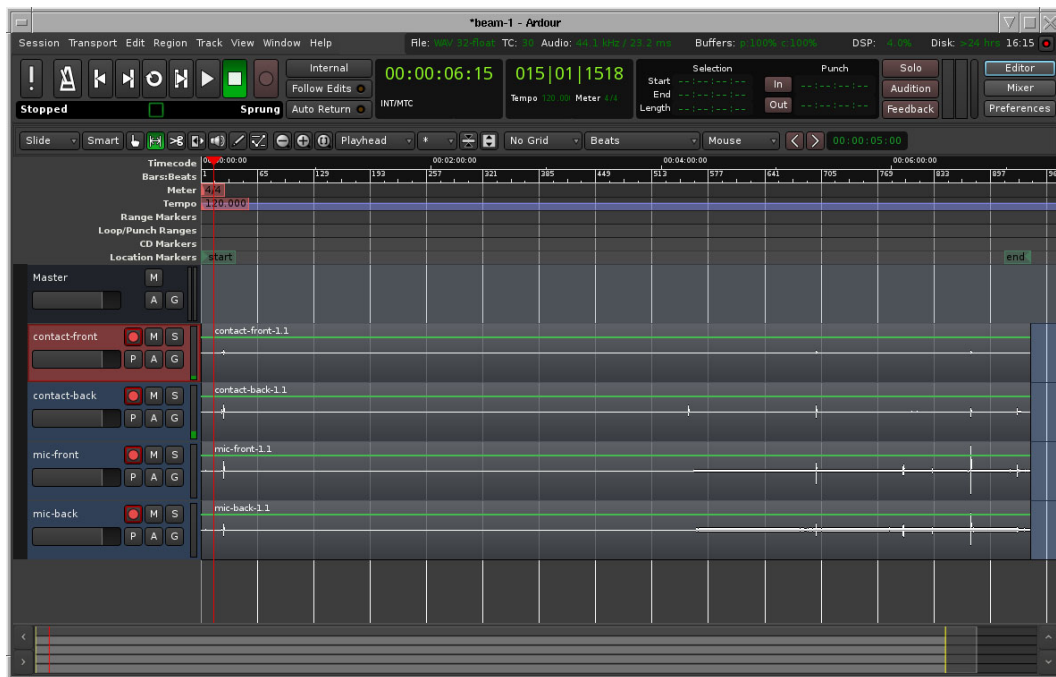


Fig. 9. An example recording of the 4 microphones shown is the entire recording for a fibre-beam (f01). At the beginning of the recording the synchronization click is visible, all other peaks belong to crack events.

4. DISCUSSION OF RESULTS

The initial results are, that in all beams fibres improve the fracture behaviour compared to SCC, although the actual post-cracking performance shows a large variability and depends on the position within the plate where the sample was taken from. Beams taken from the edges (side or end) show strain-hardening, while centre beams show strain-softening. The results coincide (roughly) with expectations from predicted fibre orientation distribution in samples, meaning that the samples where according to flow simulations the fibres should be mostly aligned in tensile stress direction, the beams show strain-hardening [28,46,47]. The high variability of results seems to be typical for small samples, where stochastic variations of density or orientation distribution matter. This means a more samples should be tested compared to non-fibre SCC. In large samples the variability should be smaller. Several draft guidelines suggest to obtain constitutive parameters from either three-point or four-point bending tests of relatively small samples, e.g., [48]. Also, in small samples the fibre orientations can be dominated by the wall-effect, leading to alignment of the fibres in the direction of tensile stresses, like in the side-edge beams taken from the plate. This could result in a strain-hardening post-cracking behaviour. If these material parameters would be chosen to design a plate, the performance of the plate could be severely overestimated.

5. ONGOING AND FUTURE INVESTIGATIONS

The analysis of fibre orientations by use of X-ray computed tomography (CT) of the tested beams has begun. Selected beams will be scanned using CT and the fibre positions and orientations will be extracted from the volume image. Special attention will be paid to the cracked region. The results of the fibre orientation measurements will be compared to computational fluid dynamics simulations of the fibre orientations. The detailed analysis regarding post-crack behaviour with respect to the location in plate is still ongoing. The relation between post-cracking strength and fibre orientations will be investigated. Comparison of peak strength and post-cracking behaviour with existing theoretical models will be performed.

6. CONCLUSIONS

In this paper the results of four-point bending tests performed on forty beam specimens cut out of a large plate have been presented. Special focus has been paid to describe the experimental setting in detail. The initial results are, that in all beams fibres improve the fracture behaviour compared to SCC, although the actual post-cracking performance depends on the

position within the plate where the sample was taken from. The results coincide (roughly) with expectations from predicted fibre orientation distribution in samples, which seems to confirm that the flow of the fresh concrete mass influences the fibre orientations. In particular, the edge beams are strain-hardening while the centre beams are strain-softening, which coincides with fibres aligned in tensile direction for the edge beams and non-aligned fibres for the centre beams. It also leads to the conclusion, that the bending results are very sensitive to the casting procedure. From this follows, that for fibre concrete specifically produced small laboratory samples may not be representative for large structural elements, this is in contrast to the case of ordinary concrete. Further, one can conclude that special care is needed to design casting technologies which will produce consistent fibre orientation distributions and that on-site casting may be problematic.

ACKNOWLEDGEMENTS

Funding by the Estonian Research Council by the exploratory research grant PUT1146 is gratefully acknowledged. Thanks to AS E-Betoonement, especially Aare Lessuk, Sergei Graf and Borys Zavadski, for preparing the experiment plates, space for cutting the beams and their general support of the research, also thanks to Ekaterina Pronyuk for being our “tourguide” on the cutting day. We also thank Elmar-Jaan Just and Peeter Linnas of the Department of Civil Engineering and Architecture, School of Engineering, for letting us use the equipment in the Mäepealse lab. The publication costs of this article were covered by the Estonian Academy of Sciences.

REFERENCES

1. Torres, A., Brandt, J., Lear, K., and Liu, J. A looming tragedy of the sand commons. *Science*, 2017, **357**(6355), 970–971.
2. Damme, H. V. Concrete material science: past, present, and future innovations. *Cem. Concr. Res.*, 2018, **112**, 5–24.
3. Suuronen, J.-P., Kallonen, A., Eik, M., Puttonen, J., Serimaa, R., and Herrmann, H. Analysis of short fibres orientation in steel fibre reinforced concrete (SFRC) using x-ray tomography. *J. Mat. Sci.*, 2012, 1–10.
4. Svec, O., Zirgulis, G., Bolander, J. E., and Stang, H. Influence of formwork surface on the orientation of steel fibres within self-compacting concrete and on the mechanical properties of cast structural elements. *Cem. Concr. Compos.*, 2014, **50**(0), 60–72.
5. Krasnikovs, A., Kononova, O., Khabbaz, A., Machanovsky, E., and Machanovsky, A. Post-cracking behaviour of high strength fiber concrete prediction and validation. *WASET*, 2011, **59**, 988–992.
6. Macanovskis, A., Lusionis, V., and Krasnikovs, A. Crack opening investigation in fiberconcrete. *WASET*, 2014, **8**(4), 430–438.

7. Laranjeira, F., Grünewald, S., Walraven, J., Blom, K., Molins, C., and Aguadoa, A. Characterization of the orientation profile of steel fiber reinforced concrete. *Mat. Struct.*, 2011, **44**(6), 1093–1111.
8. Mishurova, T., Léonard, F., Oesch, T., Meinel, D., Bruno, G., Rachmatulin, N., et al. Evaluation of fiber orientation in a composite and its effect on material behavior. In *Proceedings of the 7th Conference on Industrial Computed Tomography (ICT), Vol. 22(03), Leuven, Belgium, February 7–9, 2017*. <http://www.ndt.net/?id=20818>.
9. Eik, M., Herrmann, H., and Puttonen, J. Orthotropic constitutive model for steel fibre reinforced concrete: linear-elastic state and bases for the failure. In *Proceedings of the XII Finnish Mechanics Days, Tampere, Finland, June 4–5 (Kouhia, R., Mäkinen, J., Pajunen, S., and Saksala, T., eds)*. Finnish Association for Structural Mechanics, 2015, 255–260.
10. Eik, M., Puttonen, J., and Herrmann, H. The effect of approximation accuracy of the orientation distribution function on the elastic properties of short fibre reinforced composites. *Comp. Struct.*, 2016, **148**, 12–18.
11. Herrmann, H. An improved constitutive model for short fibre reinforced cementitious composites (SFRC) based on the orientation tensor. In *Generalized continua as models for classical and advanced materials* (Altenbach, H. and Forest, S., eds). Springer International Publishing, Switzerland, 2016, 213–227.
12. Herrmann, H. and Beddig, M. Tensor series expansion of a spherical function for use in constitutive theory of materials containing orientable particles. *Proc. Est. Acad. Sci.*, 2018, **67**(1), 73–92.
13. Vicente, M., Mínguez, J., and González, D. The use of computed tomography to explore the microstructure of materials in civil engineering: from rocks to concrete. In *Computed Tomography – Advanced Applications* (Halefoglu, D. A. M., ed.). InTech, 2017, 207–230.
14. Schnell, J., Schladitz, K., and Schuler, F. Richtungsanalyse von Fasern in Betonen auf Basis der Computer-Tomographie. *Beton-Stahlbetonbau*, 2010, **105**(2), 72–77.
15. Ponikiewski, T., Katzer, J., Bugdol, M., and Rudzki, M. X-ray computed tomography harnessed to determine 3D spacing of steel fibres in self compacting concrete (SCC) slabs. *Constr. Build. Mater.*, 2015, **74**(0), 102–108.
16. Ponikiewski, T., Katzer, J., Bugdol, M., and Rudzki, M. Steel fibre spacing in self-compacting concrete precast walls by X-ray computed tomography. *Mater. Struct.*, 2015, **48**(12), 3863–3874.
17. Pittino, G., Geier, G., Fritz, L., Hadwiger, M., Rosc, J., and Pabel, T. Computertomografische untersuchung von stahlfaserspritzbeton mit mehrdimensionalen transferfunktionen. *Beton-Stahlbetonbau*, 2011, **106**(6), 364–370.
18. Vicente, M. A., Gonzalez, D. C., and Mínguez, J. Determination of dominant fibre orientations in fibre-reinforced high-strength concrete elements based on computed tomography scans. *Nondestr. Test. Eval.*, 2014, **29**(2), 164–182.
19. Oesch, T. S., Landis, E. N., and Kuchma, D. A. Conventional concrete and uhpc performance–damage relationships identified using computed tomography. *J. Eng. Mech.*, 2016, **142**(12), 04016101.
20. Oesch, T. In-situ CT investigation of pull-out failure for reinforcing bars embedded in conventional and high-performance concretes. In *Proceedings of the 6th Conference on Industrial Computed Tomography, Wels, Austria, February 9–12, 2016*. http://www.ndt.net/article/ctc2016/papers/ICT2016_paper_id83.pdf
21. Oesch, T. S. *Investigation of fiber and cracking behavior for conventional and ultra-high performance concretes using X-ray computed tomography*. PhD thesis. University of Illinois, Urbana-Champaign, 2015.
22. Pastorelli, E. and Herrmann, H. Time-efficient automated analysis for fibre orientations in steel fibre reinforced concrete. *Proc. Est. Acad. Sci.*, 2016, **65**(1), 28–36.
23. Pastorelli, E. and Herrmann, H. Virtual reality visualization for short fibre orientation analysis. In *Proceedings of the 14th Biennial Baltic Electronic Conference (BEC), Tallinn, Estonia, October 6–8, 2014*. Institute of Electrical and Electronics Engineers, 2014, 201–204.
24. Zhang, S., Liao, L., Song, S., and Zhang, C. Experimental and analytical study of the fibre distribution in SFRC: a comparison between image processing and the inductive test. *Compos. Struct.*, 2018, **188**, 78–88.
25. Eiduks, M., Krasnikovs, A., Dunska, E., and Kononova, O. Investigation of fibre orientation in viscous fluid. *Sci. J. Riga Tech. Univ.*, 2010, **33**, 98–102. <https://ortus.rtu.lv/science/lv/publications/8346>.
26. Kononova, O., Krasnikovs, A., Lapsa, V., Kalinka, J., and Galushchak, A. Internal structure formation in high strength fiber concrete during casting. In *International Conference on Applied Mechanics and Mechanical Engineering (ICAMME 2011) Venice, Italy, November 28–30, 2011*, 1864–1867.
27. Zirculis, G., Svec, O., Geiker, M. R., Cwirzen, A., and Kanstad, T. Influence of reinforcing bar layout on fibre orientation and distribution in slabs cast from fibre-reinforced self-compacting concrete (FRSCE). *Struct. Concr.*, **17**(2), 245–256.
28. Herrmann, H. and Lees, A. On the influence of the rheological boundary conditions on the fibre orientations in the production of steel fibre reinforced concrete elements. *Proc. Est. Acad. Sci.*, 2016, **65**(4), 408–413.
29. Herrmann, H., Goidyk, O., and Braunbrück, A. Influence of the flow of self-compacting steel fiber reinforced concrete on the fiber orientations, a report on work in progress. In *Short fiber reinforced cementitious composites and ceramics* (Herrmann, H. and Schnell, J., eds). Springer, 2019, 97–110.
30. Herrmann, H., Braunbrück, A., Tuisk, T., Goidyk, O., and Naar, H. An initial report on the effect of the fiber orientation on the fracture behavior of steel fiber reinforced self-compacting concrete. In *Short fiber reinforced cementitious composites and ceramics*

- (Herrmann, H. and Schnell, J., eds). Springer, 2019, 33–50.
31. González, D. C., Vicente, M. A., and Ahmad, S. Effect of cyclic loading on the residual tensile strength of steel fiber-reinforced high-strength concrete. *J. Mat. Civ. Eng.*, 2015, **27**(9), 04014241.
 32. González, D. C., Moradillo, R., Mínguez, J., Martínez, J. A., and Vicente, M. A. Post-cracking residual strengths of fiber-reinforced high-performance concrete after cyclic loading. *Struct. Concr.*, 2018, **19**(2), 340–351.
 33. Severstal Metiz. Hendix prime 75/52 – hooked ends fiber. <http://www.severstalmetiz.ru/eng/catalogue/1930/document62190.shtml?6605,1>
 34. Pan, B., Qian, K., Xie, H., and Asundi, A. Two-dimensional digital image correlation for in-plane displacement and strain measurement: a review. *Meas. Sci. Technol.*, 2009, **20**(6), 062001.
 35. Shi, X., Pang, H., Zhang, X., Liu, Q., and Ying, M. In-situ micro-digital image speckle correlation technique for characterization of materials' properties and verification of numerical models. *IEEE Trans. Compon. Packag. Technol.*, 2004, **27**(4), 659–667.
 36. Chu, T. P. and Poudel, A. Digital image correlation techniques for aerospace applications. In *ASNT Annual Conference 2014*, 37–44.
 37. Hild, F. and Roux, S. Digital image correlation: from displacement measurement to identification of elastic properties – a review. *Strain*, **42**(2), 69–80.
 38. Andre, D. Pydic. <https://gitlab.com/damien.andre/pydic>, 2018.
 39. Grosse, C. U., Reinhardt, H. W., and Finck, F. Signal-based acoustic emission techniques in civil engineering. *J. Mater. Civ. Eng.*, 2003, **15**(3), 274–279.
 40. Wu, K., Chen, B., and Yao, W. Study on the AE characteristics of fracture process of mortar, concrete and steel-fiber-reinforced concrete beams. *Cem. Concr. Res.*, 2000, **30**(9), 1495–1500.
 41. Zhou, J. *A study of acoustic emission technique for concrete damage detection*. MSc thesis. Michigan Technological University, Department of Civil and Environmental Engineering, 2011. <https://digitalcommons.mtu.edu/etds/726>.
 42. JACK audio connection kit. <http://jackaudio.org/>
 43. Ardour5.5.0. <https://ardour.org/>
 44. Advanced Linux Sound Architecture (ALSA). <https://www.alsa-project.org>
 45. The Matplotlib Development Team. Matplotlib. <https://matplotlib.org/>
 46. Herrmann, H., Eik, M., Berg, V., and Puttonen, J. Phenomenological and numerical modelling of short fibre reinforced cementitious composites. *Meccanica*, 2014, **49**(8), 1985–2000.
 47. Eik, M., Puttonen, J., and Herrmann, H. An orthotropic material model for steel fibre reinforced concrete based on the orientation distribution of fibres. *Comp. Struct.*, 2015, **121**(0), 324–336.
 48. Walraven, J., Bigaj-van Vliet, A., et al. *fib. Model code for Concrete Structures 2010*. Wilhelm Ernst & Sohn, Verlag für Architektur und Technische Wissenschaften GmbH & Co. KG, Berlin, 2013.

Kiudude orientatsiooni mõju isetiheneva betooni 4 punkti paindetugevusele

Heiko Herrmann, Oksana Goidyk, Hendrik Naar, Tanel Tuisk ja Andres Braunbrück

Ristkülikukujuline kiudbetoonplaat lõigati neljakümneks väiksemaks talaks, millega tehti purustav 4 punkti paindekats. Katsel mõõdeti elektroonselt koormust, keskristlõike siiret ja purunemisel tekkivat akustilist emissiooni. Paralleelselt sooritati võrdluskatsed ainult betoonplaadist lõigatud katsekehadele.

Kiudbetooni katsetel täheldatud tulemuste varieeruvus paindetugevuse ja peale prao teket jääva tugevuse osas on seostatav kiudude jaotustiheduse ning orientatsioonilise jaotumisega plaadi eri piirkondades. Viimased omakorda on mõjustatud vedela kiudbetooni valuprotsessist ja -vormist.

Toodud esmaste analüüsiandmete põhjal saab väita, et laboris valatud väikeste mõõtmetega katsekehade baasil ei saa konstruktsiooniliste kiudbetoonielementide kohta järeldusi teha. Samuti vajab erilist tähelepanu kiudbetooni valuprotseduur, mille tõttu kandvate kiudbetoon-konstruktsioonide valu ehitusplatsil võib problemaatiline olla.